ACS OMEGA

http://pubs.acs.org/journal/acsodf

Article

Elongated Rodlike Particle Formation of Methyl Cellulose in Aqueous Solution

Erika Saiki, Misato Yoshida, Kei Kurahashi, Hiroki Iwase, and Toshiyuki Shikata*

Cite This: *ACS Omega* 2022, 7, 28849−28859

Read Online

ACCESS | Metrics & More | Article Recommendations | Supporting Information

ABSTRACT: The conformation and structure of methyl cellulose (MC) ether samples dissolved in pure water under dilute conditions were carefully reconsidered based on the results obtained using small-to-wide-angle neutron scattering (S-WANS), static light scattering (SLS), dynamic light scattering (DLS), and viscometric techniques. The examined MC samples possessed an average degree of substitution by methyl groups per glucose unit of ca 1.8 and weight average molar masses (M_w), ranging from 23 to 790 kg mol^{-1}. S-WANS experiments clearly demonstrated that the samples possess highly elongated rigid rodlike local structures in deuterium oxide solutions with weak periodicities of ca 0.4 and 1.0 nm on a length scale, which correspond to the average intermolecular distance between molecular chain portions facing each other in the formed rodlike structure and the repeating length of the monomeric cellobiose unit of molecular chains, respectively. Ratios of the particle length (L) to the radius of gyration (R_g) determined by SLS techniques approximately showed the relationship $LR_g^{-1} = \sqrt{12}$ holding in rigid rods over the entire M_w range examined in this study. However, the folding number, defined as the ratio of the average molecular contour length (l) to L, remained at the value of $lL^{-1} \sim 2$, representing an elongated one-folded hairpin structure, until $M_w \sim 300$ kg mol^{-1} and increased substantially up to ca 4.9 at the highest M_w of 790 kg mol^{-1}. The observed increase in the lL^{-1} value corresponded well with an increase in the diameter of the formed rod with increasing M_w observed in the S-WANS data. The M_w dependencies of the translational diffusion coefficient determined via DLS measurements and that of the intrinsic viscosity detected via viscometric techniques also distinctly demonstrated that particles formed by the MC samples dissolved in aqueous solution behave as elongated rigid rods irrespective of M_w.

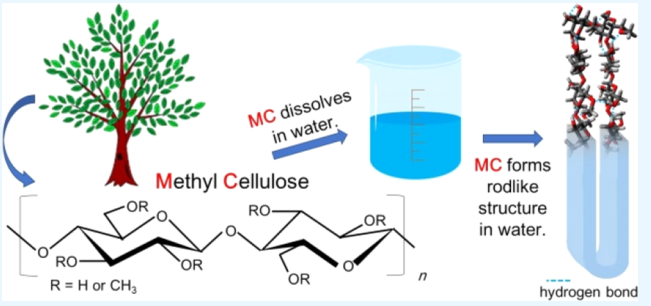

INTRODUCTION

Many kinds of plants constantly generate cellulose throughout the year. Thus, cellulose is the most abundant and steadily suppliable natural organic "biomass" resource worldwide.[1] However, native cellulose is generally insoluble in most common solvents including water. The reason for this insolubility is the highly developed inter- and intramolecular hydrogen bonds between hydroxy groups and also between hydroxy and ether groups belonging to cellulose molecular chains. Rigid stable crystalline structures called "cellulose-I$_\alpha$ and I$_\beta$" are formed by cellulose molecules in a quite efficient way in native plant cell walls, which are responsible for the insolubility in common solvents.[1−4] Although cellulose is a quite eco-friendly biomass and offers great potential as a natural resource to develop a sustainable society, its insolubility in common solvents represents an essential reason for its inapplicability to wide chemical applications in the native state. Many chemically modified cellulose derivatives which are readily soluble in various solvents have been synthesized from natural cellulose to remedy its fatal insolubility.[5] Many kinds of water-soluble chemically modified cellulose derivatives have been synthesized and supplied by several chemical manufacureers.[5,6] Methyl cellulose (MC), hydroxypropyl cellulose (HpC), hydroxypropyl methyl cellulose (HpMC), hydroxyethyl cellulose (HeC), and sodium carboxymethyl cellulose (NaCMC) ethers are typical water-soluble chemically modified cellulose derivatives, that have been widely distributed in many industries, such as those of food,[7] construction,[8] and pharmaceutical.[9,10]

Many macromolecular scientists hypothesize that most water-soluble chemically modified cellulose derivative samples have semi-flexible chain-like conformations and structures in aqueous solution and show random coil-like behavior in a sufficiently high molar mass region, similar to many ordinary synthetic polymer samples dissolved in organic solvents.[11] The literature in this field suggests that the idea of the semi-flexible or random coil-like conformation for chemically modified

Received: March 27, 2022
Accepted: July 22, 2022
Published: August 9, 2022

https://doi.org/10.1021/acsomega.2c01859
ACS Omega 2022, 7, 28849−28859

cellulose samples are simply based on the widely observed weight average molar mass (M_w) dependencies of the radius of gyration (R_g) determined by the use of static light scattering (SLS) measurements and of the intrinsic viscosity ($[\eta]$), such as $R_g \propto M_w^{\alpha}$ and $[\eta] \propto M_w^{\beta}$ with exponents of $\alpha \sim 0.6$ and $\beta \sim 0.8$, respectively, which are slightly dependent on chemically modified conditions for tested samples. However, if one examines the previously reported data[12−14] of M_w dependencies on R_g or $[\eta]$ examined over a wide M_w range very carefully, some data cannot be described by the fashion of a simple power law with only one exponent, such as $\alpha \sim 0.6$ or $\beta \sim 0.8$ over a wide M_w range. It is therefore possible that the idea of semi-flexible chain or random coil-like conformation is only prejudice to the water-soluble chemically modified cellulose samples.

Very recently, Arai et al.[15] clearly demonstrated that some water-soluble MC and HpMC ether samples, which are widely used in many industrially manufactured products, have rigid rodlike structures formed by a one-folded hairpin-like conformation of highly extended cellulose chains in M_w ranges below 100 kg mol^{-1}. They carried out small-to-wide-angle neutron scattering (S-WANS) measurements to determine the local structure of the formed particles in aqueous (deuterium oxide; D_2O) solution.[15] This striking report was the first evidence to reconsider the conformation and structure of water-soluble chemically modified cellulose samples in aqueous solutions. Bodvik et al.[16] captured evidence of the rigid rodlike structures of MC and HpMC with M_w lower than 200 kg mol^{-1} using small-angle X-ray scattering (SAXS) techniques in a low-temperature range. However, they evaluated the persistence length of 5.8 nm for both the MC and HpMC samples from their SAXS data, which meant that the molecules are semi-flexible polymer chains like the widely accepted view in cellulose derivatives.[16] Although Lodge et al.[12] also observed rigid rodlike behavior in an aqueous solution of an HpMC sample with the M_w of 370 kg mol^{-1} using SANS techniques, they mainly paid attention to the gelation mechanism of the solution. It well known that aqueous solutions of MC samples form stable gels at temperatures higher than, for example, 40 °C due to intermolecular interactions that provoke the aggregation formation of individual MC molecules into bundles having a fibril structure. The gelation mechanism is described in detail in recent reviews.[17,18]

Nevertheless, the investigated M_w range in previous studies was limited to a relatively lower range to reach the general conclusion showing the M_w dependence of conformation and structure for the MC and HpMC samples in aqueous solutions. Thus, we decided to extend the M_w range covered by experiments to lead to clear results proposing the general characteristics of the M_w dependence of conformation and structure for the same MC samples in aqueous solutions. In this study, we employ SLS techniques to precisely determine the weight average molar masses, M_w, and the radii of gyration, R_g, of the MC samples simultaneously, of which scattering vectors (q) cover a much lower range than the S-WANS techniques to provide structural information on a size scale exceeding approximately 20 nm. Thus, the conformation and structure of the MC samples are exactly determined over a wide size scale, ranging from sub-to several hundred nanometers using total curve analysis procedures for the obtained scattering functions using both the S-WANS and SLS experiments. In this study, we reached a surprising conclusion that MC molecules possibly have a rigid rodlike conformation and structure, not semi-flexible polymer chain structure, in aqueous solution over the wide M_w range examined. Then, we will report newly obtained results and conclusions below.

According to a previous report, the temperature dependencies of the hydration numbers and cloud points of MC and HpMC samples possessing similar degrees of substitution (DS) of hydroxy groups by methyl groups, ca 1.8−1.9, are substantially different.[19] Thus, it is possible that a small amount of additional substitution by hydroxypropyl groups only at the molar substitution number of MS ∼ 0.25 effectively contributes to changes in the conformation and structure of HpMC samples in aqueous solutions. In the following research, the conformation and structure of the HpMC samples will be discussed over a wide size scale range using similar total curve analysis procedures to the obtained scattering functions using both the S-WANS and SLS experiments used in this study.

Because many kinds of MC and HpMC samples, possessing similar chemically modified conditions to the samples investigated in this study, have been supplied by several chemical manufactures for wide practical applications, understanding the true conformation and structure of the samples in aqueous solution without prejudice would be helpful to reach breakthrough ideas improving processing procedures to effectively introduce solutions to the most desired flow and/or rheological conditions including processing temperatures.

EXPERIMENTAL SECTION

Materials. All MC ether samples were kindly supplied by Shin-Etsu Chemical Co., Ltd. (Tokyo). The MC samples have a constant degree of substitution (DS) of hydroxy groups per repeating $\beta(1,4)$ glucopyranose unit by methoxy (M) groups of DS = 1.8, which means the average molar mass of M_0 = 0.187 kg mol^{-1} for the repeating glucopyranose unit. The weight average molar masses (M_w) determined by SLS measurements in this study were M_w = 23, 54, 115, 206, 270, 420, and 790 kg mol^{-1}. The MC samples were coded as eg MC(1.8:23) with numerical values indicating DS and M_w/(kg mol^{-1}), respectively. All the MC samples were used for experiments without any purification procedures. The distributions of molar masses were not exceptionally sharp but rather broad as the polydispersity indices defined by ratios of M_w to the number average molar masses (M_n), $M_wM_n^{-1}$ were determined using size exclusion chromatographic techniques and reported to range from approximately 2.0 to $M_w \sim 300$ kg mol^{-1} and increased slightly with M_w values for the MC samples. Highly deionized water obtained by using a Direct-Q UV3 (Merck Milli-Q, Darmstadt) was used as a solvent to prepare sample solutions for SLS, DLS, and viscometric measurements. Deuterium oxide (D_2O) (>99.9%) was purchased from Euroisotop (Saint-Aubin) and was used as a solvent to prepare sample solution for S-WANS experiments.

The concentrations (c) of MC samples dissolved in D_2O for S-WANS measurements were set at close to the measured $[\eta]^{-1}$ values or lower than the values in aqueous solution, which are widely accepted as so-called overlapping concentrations for macromolecules in solution. The c values in the S-WANS measurements were 1.0×10^{-2} g mL^{-1} for MC(1.8:23), 1.1×10^{-3}, 2.1×10^{-3}, and 5.0×10^{-3} g mL^{-1} for MC(1.8:270), and 5.0×10^{-4} and 1.0×10^{-3} g mL^{-1} for MC(1.8:790). The c values of MC samples in pure aqueous solutions for SLS, DLS, and viscometric measurements ranged

https://doi.org/10.1021/acsomega.2c01859
ACS Omega 2022, 7, 28849−28859

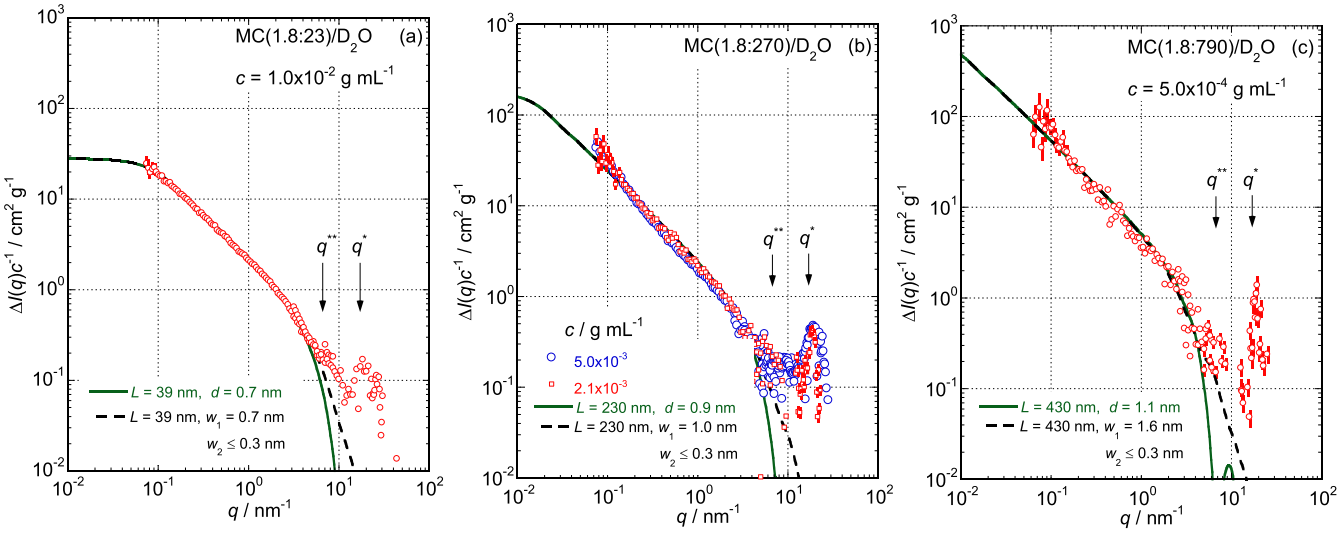

Figure 1. Dependencies of the concentration reduced excess scattering intensities, $\Delta I(q)c^{-1}$, on the scattering vector, q, for D_2O solutions of MC(1.8:23) at $c = 1.0 \times 10^{-2}$ g mL^{-1} (a), MC(1.8:270) at $c = 2.1 \times 10^{-3}$ and 5.0×10^{-3} g mL^{-1} (b), and MC(1.8:790) at $c = 5.0 \times 10^{-4}$ g mL^{-1} (c) in the S-WANS experiments at 25 °C. Solid and broken lines indicate the fit theoretical form factors, $P(q)$ calculated using SasView,[22] for rods and rectangular columns with the size parameters shown in each figure on the scale of nanometer.

from 3×10^{-4} to 6×10^{-2} g mL^{-1} depending on the sample M_w values.

Methods. S-WANS measurements were carried out at Materials and Life Science Experimental Facility (MLF) in Japan Proton Accelerator Research Complex, J-PARC, (Tokai) using a small-angle neutron scattering instrument (TAIKAN)[20] installed on a beamline BL15. The magnitude of the scattering vector (q) covered by the S-WANS experiments ranged from 7.0×10^{-2} to 1.0×10^{2} nm^{-1}. Square-type quartz cuvettes with a neutron beam path length of 4.0 mm or banjo-type quartz cuvettes with a path of 2.0 mm were used as sample cells. The standard exposure time was 2 h for each sample solution. S-WANS measurements were carried out at 25 °C. The obtained scattering data were converted to absolute values using the standard material "glassy carbon" for which absolute scattering values had been precisely determined.

SLS and DLS measurements were carried out using a modified DLS7000 (Otsuka Electronics Co. Ltd., Osaka). A continuous-wave solid-state single-frequency laser at a wavelength of λ = 488.0 nm, Sapphire SF488-100 (Coherent, Inc., Santa Clara), was equipped with the modified DLS7000 and was used as a light source for SLS and DLS measurements. A photomultiplier, R9880U-01 (Hamamatsu Photonics K. K., Hamamatsu), was used as a scattered light intensity detector. An LSI correlator (LS Instrument AG, Fribourg) was used to record fluctuations in scattered light intensity as a function of time and to create an autocorrelation function of the scattered light intensity. A Pyrex glass tube with an inner diameter and thickness of 19.0 and 0.5 mm, respectively, was used as a measuring cell. The measuring temperature was set at 25.0 °C, and the scattering angle (θ) was altered from 30 to 150° every 10° step. The magnitude of the scattering vectors, which is given by the equation $q = |\boldsymbol{q}| = (4\pi n/\lambda)|\sin(\theta/2)|$, where n is the refractive index of water, ranged from 8.86×10^{-3} to 3.31 $\times 10^{-2}$ nm^{-1} for both the SLS and DLS measurements. Toluene was used as the standard liquid material for scattered light intensities at each θ in the SLS measurements. The refractive index increment (dn/dc) of the MC samples was determined to be 0.134 mL g^{-1} using an Abbemat MW multiwavelengths refractometer (Anton Paar, Graz) at a wavelength of λ = 486 nm. Because the value of dn/dc = 0.133 mL g^{-1} was also obtained at λ = 589 nm^{-1}, the λ dependence of dn/dc was quite weak.

The intrinsic viscosities, $[\eta]$, for each MC and HpMC sample in aqueous solution were determined at 25.0 °C using an Ubbelohde-type capillary viscometer.

RESULTS AND DISCUSSION

S-WANS Behaviors for MC Samples. An excess value in the scattering intensity of a solution sample $[I(q)]$ with respect to that of the solvent $[I_{solv}(q)]$ and a small q independent incoherent component (I_{incoh}) was normalized by the concentration, c, to obtain the characteristic scattering intensity, $\Delta I(q)c^{-1} = (I(q) - I_{solv}(q) - I_{incoh})c^{-1}$, for each tested sample. Some S-WANS behaviors such as the q dependence of $\Delta I(q)c^{-1}$, observed in MC sample solutions, are shown in Figure 1a–c with the evaluated error bars to show the accuracy of the experiments. Because the concentration, c, for each MS sample was not higher than the so-called overlap concentration, $c^* = [\eta]^{-1}$, S-WANS behaviors are almost independent of c and reflect the isolated state in D_2O solutions. In the case of the behavior for MC(1.8:23) with the lowest M_w in the examined MC samples, $\Delta I(q)c^{-1}$ data seem to have a plateau region in a q range lower than 0.1 nm^{-1}, an inversely proportional region showing the relationship $\Delta I(q)c^{-1} \propto q^{-1}$ in a q range of 0.1 nm^{-1} < q < 3.0 nm^{-1}, and a steeply decreasing region with q values showing a couple of characteristic interference scatterings, as seen in Figure 1a. The presence of a plateau region in the $\Delta I(q)c^{-1}$ data means that MC(1.8:23) molecules have a characteristic size not far from 10 nm. On the other hand, the relationship $\Delta I(q)c^{-1} \propto q^{-1}$ strongly suggests a rigid rodlike structure for the sample. The broad interference scatterings observed at $q^* \sim 17$ and $q^{**} \sim 6$ nm^{-1}, which correspond to the spacing distances of $\delta^* \sim 0.4$ and $\delta^{**} \sim 1.0$ nm, indicate the presence of loose periodicities in the rigid rodlike structure. There is a broad peak in the S-WANS data of solvent D_2O at q = 20 nm^{-1}, which corresponds to 0.3 nm in scale. Because the observed peak value of q^* = 17 nm^{-1} was

https://doi.org/10.1021/acsomega.2c01859
ACS Omega 2022, 7, 28849−28859

slightly smaller than the peak q value of D_2O and the q dependence of the interference peak observed at q^* was obviously sharper than that of D_2O, we concluded that the observed peaks at q^* result from the periodic structure formed in the particles of MC molecules dissolved in water.[15]

A solid curve drawn in Figure 1a reveals a theoretically calculated q dependence of the form factor ($P(q)$) of a rigid rod[21] with a length and diameter of L = 39 and d = 0.7 nm, respectively, which was calculated using SasView[22] multipurpose open source software for small-angle scattering data analysis and multiplied by a certain adequate value to fit the q dependence of the data. The reason for the L value is described in the later section. Reasonable agreement between the solid curve and $\Delta I(q)c^{-1}$ data convincingly reveals that the MC(1.8:23) molecules have a rigid rod shape with L = 39 and d = 0.7 nm in aqueous solution. Essentially, the same S-WANS behavior except for the presence of a plateau $\Delta I(q)c^{-1}$ region has already been observed in the S-WANS behaviors in the samples of MC(1.8:54) and MS(1.8:115) with M_w higher than MC(1.8:23) in the previous report,[15] which are well described by the form factors of rigid rods with the same d value of 0.8 nm and L values longer than 39 nm. Briefly stated, the form factor of a rigid rod, $P(q)$, with L and d exhibits a plateau value ca unity in the q range less than ca $(L/3)^{-1}$ and is followed by the characteristic relationship $P(q) \propto q^{-1}$ up to a q value ca $(d/3)^{-1}$, then decreases rapidly above the q value. The broken line in Figure 1a indicates the q dependence of the theoretical form factor, $P(q)$, of a rectangular cuboid (rectangular column) calculated by SasView[22] with L = 39 nm and major and minor widths of w_1 = 0.7 and w_2 = 0.3 nm, respectively. Since this form factor for the rectangular column is hardly distinguishable from that for the rod, a rectangular column is also a likely candidate for the structure of MC(1.8:23) molecules in aqueous solution.

Figure 1b,c represents the q dependence of $\Delta I(q)c^{-1}$ data for MC(1.8:270) and MC(1.8:790), respectively, possessing much higher M_w values than MC(1.8:23). In the case of the MC(1.8:270) sample, the c^* value is calculated to be 1.9×10^{-3} g mL^{-1}, whereas $\Delta I(q)c^{-1}$ data obtained at $c = 5.0 \times 10^{-3}$ g mL^{-1}, which is approximately 2.6 times as high as c^*, appear to follow those determined at c lower than c^* even in a low q range. Basically, the essential rigid rod particle characteristics also remain in these longer MC samples in a local structure covered by the S-WANS behaviors. However, a steep decrease in the $\Delta I(q)c^{-1}$ data starts at $q \sim 1.5$ nm^{-1}, which is slightly lower than that of MC(1.8:23). Since the solid lines in Figure 1b,c represent the q dependencies of the form factors, $P(q)$, of rigid rods with d = 0.9 and L = 230 nm, and d = 1.1 and L = 430 nm, respectively, calculated using SasView,[22] and reasonably fit the $\Delta I(q)c^{-1}$ data, the essential reason for the decrease in $\Delta I(q)c^{-1}$ at lower q values than the MC(1.8:23) sample seems to be an increase in the d value with increasing M_w. These L values are determined in the later section. Agreement between $\Delta I(q)c^{-1}$ data and theoretical form factors for rectangular columns with w_1 = 1.0 and $w_2 \leq 0.3$ nm, as seen in Figure 1b, and w_1 = 1.6 and $w_2 \leq 0.3$ nm, as seen in Figure 1c, is also recognized in the S-WANS behavior as well as that of rods. Any w_2 values smaller than 0.3 nm provided the form factor, $P(q)$, which was essentially the same as that obtained with w_2 = 0.3 nm in a q range less than 15 nm, for rectangular columnar particles with the fixed L and w_1 values. Although one cannot determine which model is more suitable to describe the structure of MC molecules in aqueous solution, the enlargement of the cross-sectional dimension for rodlike particles formed by MC molecules in aqueous solution with increasing M_w values is indubitable.

Chatterjee et al.[23] carried out SANS experiments in D_2O solutions of MC samples with M_w = 410 and DS = 1.9, and with M_w = 53 kg mol^{-1} and DS = 1.8 to investigate the gelation mechanisms of MC samples in aqueous solutions. They clearly observed the $\Delta I(q) \propto q^{-1}$ behavior in a q range from 1.0×10^{-1} to 1.0 nm^{-1} at temperatures such as 5.8 and 10.9 °C, which were sufficiently lower than gelation temperatures of 43.6 and 57.4 °C, respectively, for the MC samples, as seen in Figure 1a,b. However, they also observed the behavior of $\Delta I(q) \propto q^{\sim -2.5}$ in a lower q range from 1.0×10^{-2} to 5.0×10^{-2} nm^{-1} in both systems. Although the reasons for such stronger q exponents in their SANS data are not clear at present, the MC sample concentration of $c = 1.5 \times 10^{-2}$ g mL^{-1} in their experiments is substantially higher than the overlapping concentrations, c^*, between MC molecules. The q dependence of structure factors controlled by the interactions between MC molecules at the (not sufficiently low) concentrations would thus be one of the essential reasons for the observed stronger q exponents. Because the SLS experiments cover a q range from 8.86×10^{-3} to 3.31×10^{-2} nm^{-1} under dilute conditions without the effects of molecular overlap, the exact q dependence of form factors, $P(q)$, for isolated MC molecules describing the overall structure and conformation in aqueous solution will be discussed in detail later.

It is noteworthy that the $\Delta I(q)c^{-1}$ value of the MC(1.8:790)/D_2O system, ca 5.0 cm^2 g^{-1}, is substantially greater than those of the MC(1.8:23)/D_2O, ca 2.0 cm^2 g^{-1}, and MC(1.8:270)/D_2O, ca 2.5 cm^2 g^{-1}, systems at a constant q value of 1.0 nm^{-1}, as seen in Figure 1. If rod particles dissolved in D_2O possess the same diameter, d, and different particle lengths, L, the q dependence of $\Delta I(q)c^{-1}$ value does not depend on L (or M_w) in a q range sufficiently higher than L^{-1}. The fact that the $\Delta I(q)c^{-1}$ values for the different MC samples at q = 10 nm^{-1} ($\ll L^{-1}$) are not identical to one another, as seen in Figure 1, suggests the variation of d (or w_1) depending on the M_w values especially for the high M_w MC samples examined in this study such as MC(1.8:790).

Because the $\Delta I(q)c^{-1}$ data obtained at c values lower than c^* are poorly scattered, as shown in Figure 1b,c, the presence of broad interference peaks at $q^{**} \sim 6.0$ nm^{-1} is not obvious. However, the $\Delta I(q)$ data for MC(1.8:270) at $c = 1.0 \times 10^{-2}$ g mL^{-1} clearly demonstrate the existence of the two peaks at the q values identical to that for MC(1.8:23), as seen in Figure 1a. The highly extended conformation of MC molecular chains demonstrating a spacing, δ^{**}, related to the repeating distance of cellobiose of ca 1.0 nm corresponds to q^{**}.[15] The distance between two MC molecular chain portions facing each other due to the folding structure formed by the hydrogen bonds between the remaining hydroxy groups, as schematically depicted in Figure 2a, corresponds well to another periodic spacing, δ^*, related to q^* in MC samples possessing lower M_w value than ca 100 kg mol^{-1}.[15] Intermolecular periodicities close to 0.4 nm are usually observed in the reported crystalline structure of cellulose II.[24] Because these interference peaks were always observed irrespective of the M_w values, the hairpin-like structure seems to be a fundamental conformation for the MC molecules in aqueous solution for all the samples examined.

https://doi.org/10.1021/acsomega.2c01859
ACS Omega 2022, 7, 28849−28859

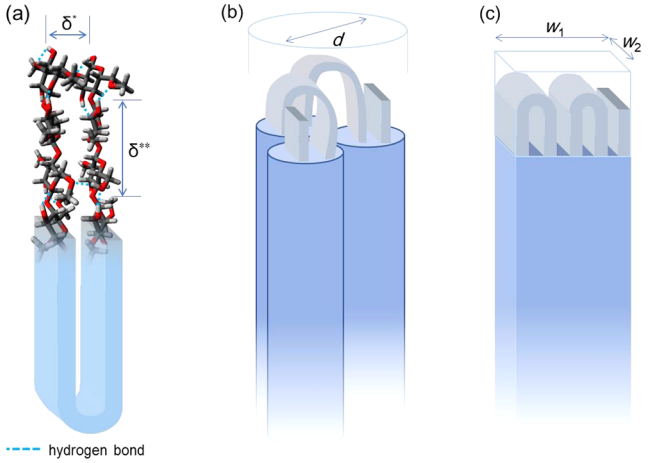

Figure 2. Schematic depiction of the particle structure possibly formed by the MC samples in aqueous solution: a one-time folded hairpin-type particle in a lower M_w range (a), a randomly coagulated bundle structure of hairpin-like parts in parallel with $lL^{-1} = 6$ (b), and a sequential two dimensional array of hairpin-like parts formed by a highly extended molecular chain with $lL^{-1} = 5$ (c). Small rectangular columns constructing each large particle described in (b,c) represent extended molecular chain parts of MC molecules seen in (a).

The cross-sectional enlargement of the formed rodlike structure with increasing M_w results from the increasing molecular chain numbers per the cross section of the formed particles, that is, bundle formation of hairpin-like parts. In the next section, we will determine a ratio between the average molecular contour length (l) and the average particle length (L), lL^{-1}, for each MC sample, assuming the rigid rod model.[15] The determined lL^{-1} value starts from approximately 2 at lower M_w values and increases up to 4.9 at the highest value of M_w = 790 kg mol^{-1}. These results strongly support the one-folded hairpin-like particle structure formation of highly extended molecular chains, as seen in Figure 2a, for MC samples with low M_w values.[15] Very recently, the formation of a two dimensional array of hairpin-like parts to construct highly elongated rectangular columnar particles similar to the structure, as seen in Figure 2c, was also found in poly(vinylidene fluoride) (PVDF) solution dissolved in *N*-methylpyrrolidone (NMP).[25] Referring the particle structure formed by PVDF molecules, we speculate that the increase in the lL^{-1} ratio with increasing M_w leads to at least two possible developments in the formed particle structure: a randomly coagulated bundle structure of a couple of hairpin-like parts in parallel formed by a highly extended molecular chain with some folding points, as schematically depicted in Figure 2b, and a sequential two-dimensional array of hairpin-like parts formed by a highly extended molecular chain, as seen in Figure 2c. The former structure corresponds to the rodlike structure, and the latter corresponds to the rectangular columns assumed above. When the interaction between the formed hairpin-like parts is not so strong as to form the sequential two dimensional arrays shown in Figure 2c, randomly coagulated bundles, as seen in Figure 2b, will be constructed. The reason for the formation of bundles of hairpin-like parts, as seen in Figure 2b,c, is the hydrophobic interactions and hydrogen bond formation between the parts using the remaining hydroxyl groups on the MC molecular chains. The hydrophobic interaction is also important for intermolecular associative behavior of MC molecules in aqueous solution related to the gelation mechanisms of aqueous MC systems.[26]

Rodlike particles are formed by isolated MC molecules at 25 °C in dilute aqueous solutions, as described in this study. Isolated rodlike MC particles would gather into bundles to make long fibrils due to the hydrophobing of the surface of MC rodlike particles and also interparticle hydrogen bond formation caused by the dehydration of MC molecules at higher temperatures than, for example, 40 °C, as proposed by previous studies.[17,18,26] When the formed long fibrils of MC molecules contact each other at high temperatures, the contact points will result in cross-linking points inducing the gelation of the systems due to the hydrogen bond formation.

SLS Behaviors. To probe structure of particles formed by MC molecules on the scale larger than that covered by the S-WANS experiments, SLS measurements were quite useful. The excess Rayleigh ratios (R_θ) from the solvent, water, were determined at each θ in the SLS measurements. The optical constant (K) of the SLS apparatus was determined using a dn/dc value of 0.134 mL g^{-1}. As the distributions of the molar masses of the investigated MC and HpMC samples were not exceptionally sharp, the so-called Berry plot,[27,28] $\sqrt{KcR_\theta^{-1}}_{c=0}\left(=\lim_{c\to 0}\sqrt{KcR_\theta^{-1}}\right)$ versus q^2 and $\sqrt{KcR_\theta^{-1}}_{q=0}\left(=\lim_{q\to 0}\sqrt{KcR_\theta^{-1}}\right)$ versus c, was used to determine the weight average molar masses, M_w, and the radii of gyration, R_g, of the samples instead of the Zimm plot.[29] The Berry plots obtained for aqueous solutions of MC(1.8:270) are shown in

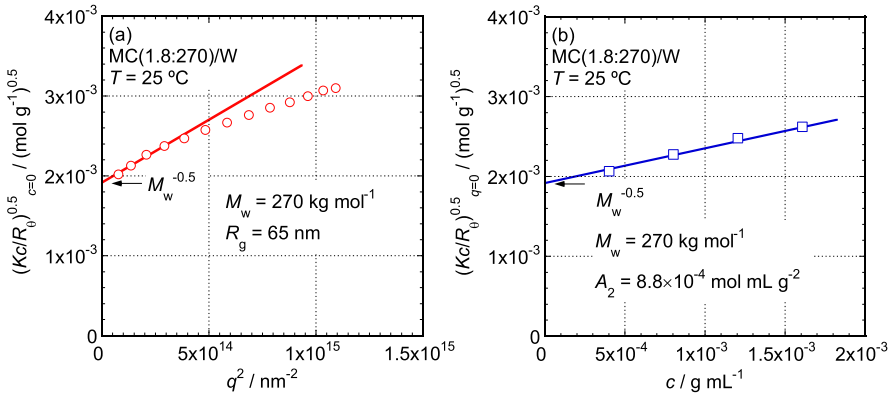

Figure 3. Dependencies of $\sqrt{KcR_\theta^{-1}}_{c=0}$ data on q^2 (a) and $\sqrt{KcR_\theta^{-1}}_{q=0}$ on c (b) for aqueous solutions of MC(1.8:270) at 25 °C.

https://doi.org/10.1021/acsomega.2c01859
ACS Omega 2022, 7, 28849−28859

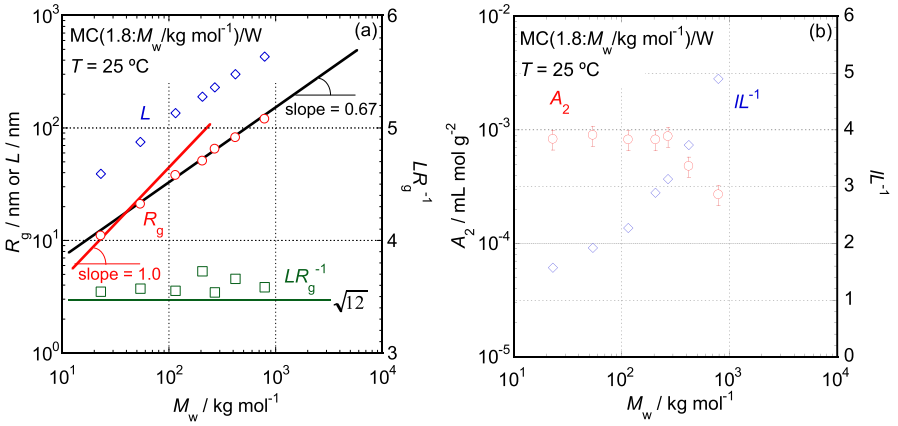

Figure 4. Dependencies of R_g, L, and LR_g^{-1} on M_w (a) and A_2 and lL^{-1} on M_w (b) for aqueous solutions of the MC samples at 25 °C.

Figure 3 as typical results. The processes in which $\sqrt{KcR_\theta^{-1}}_{c=0}$ and $\sqrt{KcR_\theta^{-1}}_{q=0}$ data were determined are summarized in the Supporting Information, S1. According to the standard method, because the intercept and initial slope of a straight line found in Figure 3a indicate the values of $1/\sqrt{M_w}$ and $R_g^2/(6\sqrt{M_w})$, respectively, M_w and R_g can be determined to be 270 kg mol^{-1} and 65 nm, respectively. The straight line obviously deviates from the $\sqrt{KcR_\theta^{-1}}_{q=0}$ data in a high q range, as observed in Figure 3a. On the other hand, from the intercept of a straight line shown in Figure 3b indicating $M_w^{-0.5}$, the value of M_w = 270 kg mol^{-1} was confirmed. Moreover, the second Virial coefficient (A_2) can be obtained as 8.8 × 10^{-4} mol mL g^{-2} from the slope of a straight line, as seen in Figure 3b, since the slope theoretically represents the value of $A_2M_w^{0.5}$. According to the same procedures, the values of M_w, R_g, and A_2 were determined for each MC sample.

Figure 4a shows the M_w dependence of R_g for the MC samples in aqueous solution. If one would like to approximately describe the relationship between the parameters using a simple power law, such as $R_g \propto M_w^{\alpha}$, an M_w exponent, α, could be determined to be ca 0.67. This value is typical for slightly expanded flexible polymer chains in solution.[23] However, the validity of the simple power law seems to be doubtful because the R_g data points seem to have a tendency to increase the slope gradually in a low M_w side, as seen in Figure 4a. In particular, the data points on the lower M_w side show the relationship $R_g \propto M_w$, which means that the MC molecules with M_w values lower than ca 100 kg mol^{-1} simply behave as rigid rods in aqueous solution. The widely accepted idea that water-soluble MC samples behave as semiflexible or random coil-like polymer chains at sufficiently high M_w should be reconsidered, considering the S-WANS experimental fact demonstrating an increase in the diameter of the local rigid-like structure with increasing M_w, as discussed above.

A substantial decrease in the A_2 data observed at a higher M_w than ca 300 kg mol^{-1}, as seen in Figure 4b, means a decrease in repulsive interparticle interactions, and in other words, an increase in attractive interparticle interactions.[27−29] It is interesting to note that the proportional relationship observed between R_g and M_w starts to deviate downwardly in an M_w range similar to that for the beginning of a decrease in the A_2 value, as determined from Figure 4a,b.

Here, we analyze the overall shape of MC molecules in aqueous solution employing a rigid rod particle model[21] and a rectangular columnar model[30] based on the obtained q dependencies of $[R_\theta(Kc)^{-1}]_{c=0}$(= $\lim_{c\to 0} R_\theta(Kc)^{-1}$) data that were calculated from the intercepts of Berry plots; $[R_\theta(Kc)^{-1}]_{c=0} = (\lim_{c\to 0}\sqrt{KcR_\theta^{-1}})^2$. Because the relationship $[R_\theta(Kc)^{-1}]_{c=0} = M_wP(q)$ holds theoretically, the q dependence of $[R_\theta(Kc)^{-1}]_{c=0}$ essentially represents that of the particle form factor, $P(q)$. Consequently, if one finds the correct particle form factor, $P(q)$, agreement between $[R_\theta(Kc)^{-1}]_{c=0}$ data and $M_wP(q)$ would be confirmed over the entire q range covered by both SLS and S-WANS techniques. In curve fit procedures of the $M_wP(q)$ to $[R_\theta(Kc)^{-1}]_{c=0}$ data, assuming the rigid rod and rectangular columnar models, the multipurpose software, SasView, was used again.

The determined best fit $M_wP(q)$ curves for each MC sample are shown in Figure 5. The particle lengths, L, necessary to describe the best fit $M_wP(q)$ curves are also summarized in Table 1 with the estimated uncertainty of ±5%. The diameters, d, for rods and widths, w_1 and w_2, for rectangular columns used to calculate the best fit form factors, $P(q)$, were the values that

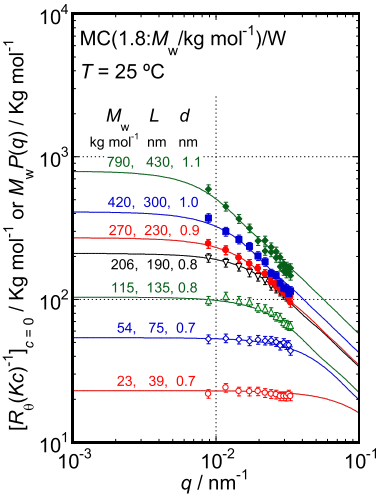

Figure 5. Dependencies of $[R_\theta(Kc)^{-1}]_{c=0}$(= $\lim_{c\to 0} R_\theta(Kc)^{-1}$) data and $M_wP(q)$ on q for aqueous solutions of the MC samples at 25 °C. The assumed diameters, d, for the rod models are shown in the figure.

https://doi.org/10.1021/acsomega.2c01859
ACS Omega 2022, 7, 28849−28859

Table 1. Codes, the Weight Average Molar Masses, M_w, the Radii of Gyration, R_g, the Particle Length, L, the Contour Length, l, the Ratio of l/L, the Particle Diameters, d, the Particle Major and Minor Widths, w_1 and w_2, the Translational and Rotational Diffusion Constants, D_t and D_r, the Intrinsic Viscosity, $[\eta]$, and the Hydrodynamic Radii, R_h, for the Examined MC Samples

code	M_w/kg mol^{-1}[a]	R_g/nm[a]	L/nm[a]	l/nm	l/L	d/nm	w_1/nm	w_2/nm	D_t/m^2 s^{-1}	D_r/s^{-1}	R_h/nm	$[\eta]$/mL g^{-1}
MC(1.8:23)	23.0	11	39	61.4	1.6	0.7[a]	0.7[a]	≤0.3	5.2 × 10^{-11}		4.7	44.0
MC(1.8:54)	54.0	21	75	144	1.9	0.7[a]	0.7[a]	≤0.3	3.1 × 10^{-11}		7.9	130
MC(1.8:115)	115	38	135	306	2.3	0.8[a]	0.8[a]	≤0.3	2.0 × 10^{-11}		12	260
MC(1.8:206)	206	51	190	550	2.9				1.6 × 10^{-11}		16	360
MC(1.8:270)	270	65	230	720	3.1	0.9[b]	1.0[b]	≤0.3	1.2 × 10^{-11}	2.0 × 10^3	20	530
MC(1.8:420)	420	82	300	1120	3.7				1.0 × 10^{-11}	1.1 × 10^3	25	610
MC(1.8:790)	790	120	430	2110	4.9	1.1[c]	1.6[c]	≤0.3	7.0 × 10^{-12}	3.3 × 10^2	35	840

[a]Containing the uncertainty of ±5%. [b]Containing the uncertainty of ±7%. [c]Containing the uncertainty of ±10%.

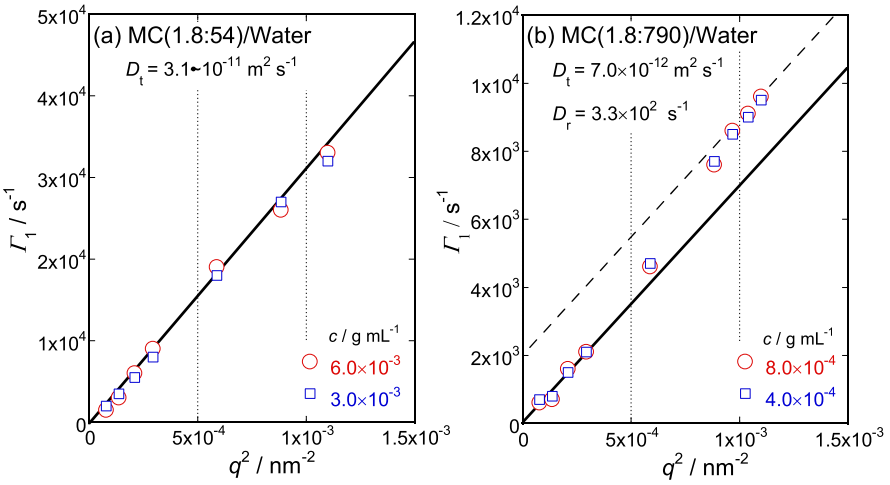

Figure 6. Dependencies of the first cumulants, Γ_1, on q^2 for aqueous solutions of MC(1.8:54) (a) and MC(1.8:790) (b).

had been determined and are summarized in Table 1 in the S-WANS data analysis section above to discuss the local structure of the formed particles. In fact, if one uses particle diameter and width values that are a few times greater than the values shown in Table 1 to calculate $M_wP(q)$ curves, their q dependencies observed in the q range covered by the SLS measurements do not change at all. We only show the q dependencies of the $M_wP(q)$ curves calculated with d values, as seen in Table 1. The reasonable agreement between the $[R_\theta(Kc)^{-1}]_{c=0}$ data with error bars and $M_wP(q)$ curves, as seen in Figure 5, assuming the rigid rod model for all the MC samples, strongly suggests that MC molecules construct particles possessing elongated rigid rodlike conformations and structures in aqueous solutions over the entire range of examined M_w values.

Figure 4a also shows the M_w dependence of the ratio of LR_g^{-1}, which is roughly described to be a constant value close to 3.5 irrespective of the M_w values. Because the relationship $L^2 = 12R_g^2$ ($\sqrt{12} = 3.46$) holds for rigid long rods, the fact that $LR_g^{-1} \sim 3.5$ reveals that the MC samples behave as rigid rods in aqueous solution irrespective of the M_w values from the SLS behavior viewpoint.[22] However, we must emphasize another important folding characteristic in the MC molecules related to an increase in the diameters of the formed rigid rod particles with increasing M_w (cf Table 1 and Figure 2). Because the repeating length of the fundamental glucopyranose unit has been known to be ca 0.5 nm, one can calculate the weight average molecular contour length, l, of MC molecules from their M_w values. In accordance with the folding structure of elongated MC molecule chains schematically depicted in Figure 2, a folding number for MC molecules is determined as lL^{-1}, which represents "the average number of MC molecular chains per cross section" of the formed MC particles in aqueous solution. The dependence of the folding number, lL^{-1}, on the M_w value is also plotted in Figure 4b. Because the lL^{-1} values seem to maintain a constant value of ca 2 in a M_w range lower than 100 kg mol^{-1} and show steep increase with increasing M_w, the increase in diameter of the formed rigid rods or rectangular columns clearly results from that in the lL^{-1} values. Therefore, although the MC samples show a change in folding number, lL^{-1}, with increasing M_w, they maintain their rigid rodlike or rectangular column-like structure over the entire range of examined M_w values.

The examined MC samples demonstrate cloud points, for example, 37 °C significantly lower than those of other water-soluble chemically modified cellulose samples. The small A_2 values of the MC samples with high M_w observed in this study suggest relatively strong attractive interparticle interactions. It is likely that these observations are induced by the characteristics of the formed rodlike particles. Fortunately, the curve fit analysis could be successfully applied to all the MC samples examined in this study. However, it is possible that the analysis cannot be applied MC samples with $M_w > 10^3$ kg mol^{-1} due to the non-negligible contribution of flexibility in the formed particles, even if rodlike shape particles are formed in the MC samples.

DLS Behaviors. The autocorrelation function of the light electric field ($\boldsymbol{E}$ ($\boldsymbol{q}$, t)) scattered by dispersed particles in a liquid medium as functions of scattering vector, $\boldsymbol{q}$, and time (t) defined as $g_1(t) = \langle E^*(\boldsymbol{q},0)E(\boldsymbol{q},t)\rangle$, where the asterisk indicates

https://doi.org/10.1021/acsomega.2c01859
ACS Omega 2022, 7, 28849−28859

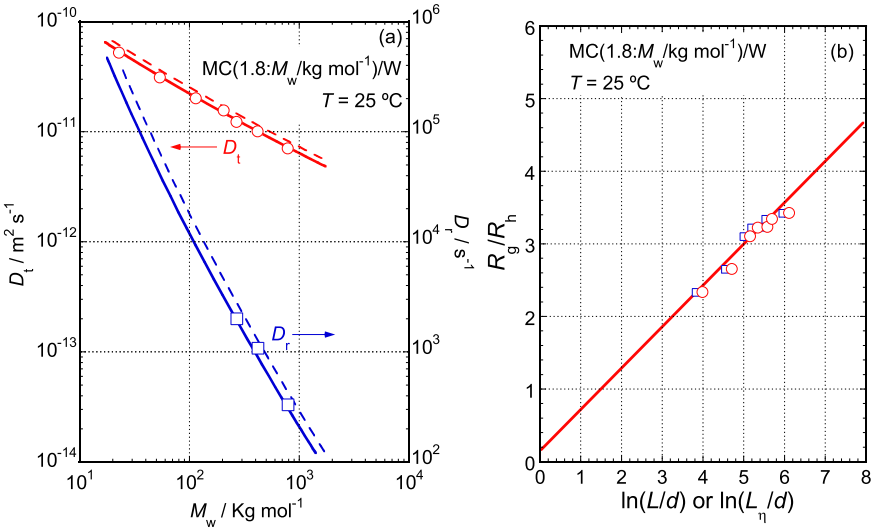

Figure 7. (a) Dependencies of the translational, D_t, and rotational diffusion coefficient, D_r, on M_w and (b) dependence of the shape factor, ρ, on ln(L/d), circles, or ln(L_η/d), squares, for the MC samples dissolved in aqueous solution. Solid lines represent theoretical calculations, and broken lines mean theoretical calculations, assuming the hydrodynamic particle length $L_\eta = 0.85L$ in (a).

complex conjugate, is related to the autocorrelation function of the light intensity ($I(\boldsymbol{q}, t)$) scattered by dispersed particles defined as $g_2(t) = \langle I(\boldsymbol{q},0)I(\boldsymbol{q},t)\rangle$ via the so-called Siegert equation given by $g_2(t) = 1 + a|g_1(t)|^2$, where a represents a certain constant value depending on the apparatus used.[31] According to the standard DLS theory, the first cumulant of $g_1(t) = \sqrt{(g^2(t) - 1)/a}$ defined as $\Gamma_1 = -\lim_{t\to 0} \partial \ln g_1(t)/\partial t$ is directly related to the average translational diffusion coefficient (D_t) of the dispersed particles in the liquid medium in the manner of $\Gamma_1 = q^2 D_t$.[31] This consideration is valid only for smaller particles with characteristic sizes less than q^{-1}. In the case of larger anisotropic particles such as rods, one should use the relationship $\lim_{q^2\to 0} \Gamma_1 = q^2 D_t$ to evaluate D_t values precisely because the contribution of rotational diffusion processes of particles cannot be ignored in a higher q range.

Figure 6a,b demonstrates the typical q^2 dependencies of the obtained first cumulants, Γ_1, for the short MC(1.8:54) and the longest MC(1.8:790) samples, respectively. Although the Γ_1 data of MC(1.8:54) have a constant slope showing a D_t value ca 2.9 × 10^{-11} m^2 s^{-1} over the entire q^2 range examined irrespective of the concentration, c, that of MC(1.8:790) seems to have two straight parts. D_t can be evaluated from the initial slope, $\lim_{q^2\to 0} \Gamma_1/q^2$, of the Γ_1 data to be D_t = 7.0 × 10^{-12} m^2 s^{-1} for MC(1.8:790). In addition to this initial proportional part, the Γ_1 data of MC(1.8:790) possess the second straight part, which has the identical slope to the D_t value, in a higher q^2 range, as seen in Figure 6b. Berne et al.[31] suggested that the intercept of an extrapolation of the straight part of the Γ_1 data found in higher q^2 range provides six times the rotational diffusion coefficient (D_r) for large anisotropic particles. Some experimental results verified this idea.[32−34] According to them, the D_r value can be evaluated to be 3.3 × 10^2 s^{-1} for MC(1.8:790) from the intercept of a broken straight line, as seen in Figure 6b. In all the MC samples, the D_t values could be determined from the (initial) slopes of the Γ_1 data, whereas the D_r values were determined only for the longest three MC samples. Although depolarized dynamic light scattering (DLS) experiments[31] are known as the most reliable method to determine D_r values for particles with anisotropic structures and were tried in this study, the observed scattering intensities under the depolarized condition were too low to determine D_r values in the aqueous solutions of MC samples examined in this study. All the determined D_t and D_r values and the hydrodynamic radii (R_h) calculated from the D_t values using the Stokes-Einstein relationship, $R_h = k_B T(6\pi\eta_w D_t)^{-1}$, where k_B, T, and η_w are the Boltzmann constant, the absolute temperature, and water viscosity, are also summarized in Table 1.

The obtained M_w dependencies of the D_t and D_r values are shown in Figure 7. The D_t value decreases with increasing M_w, approximately demonstrating the relationship $D_t \propto M_w^{-0.5}$, as usually observed for many flexible polymers in solutions. However, the so-called shape factor ($\rho = R_g/R_h$) for the MC samples, which approximately shows proportionality to ln(L/d), as clearly seen in Figure 7b, is greater than that for flexible polymer chains such as the constant value of ca 1.56 in good solvents. According to the theoretical consideration, ρ can be described with an equation $\rho = 0.18 + 0.58\ln(L/d)$ for long rods with the ratio of $L/d > 10$, which is shown in Figure 7b.[35] Agreement between the theory and experimental ρ data appears to be reasonable. This consideration of the shape factor, ρ, strongly demonstrates that the particles formed in the aqueous solutions of the MC samples behave as rigid elongated rodlike particles.

Here, we discuss the M_w dependencies of D_t and D_r based on the rigid rod particle model. Ortega and García de la Torre[35] proposed simple expression methods for theoretical D_t and D_r including numerical parameters as follows.

$$D_t = \frac{k_B T\{\ln(L/d) + C_t\}}{3\pi\eta_w L} \quad (1)$$

$$D_r = \frac{3k_B T\{\ln(L/d) + C_r\}}{\pi\eta_w L^3} \quad (2)$$

where C_t and C_r are the numerical factors described by polynomials of the ratio of L/d.[35] The solid and broken lines observed in Figure 7a represent the M_w dependencies of theoretically calculated D_t and D_r, respectively, substituting the

https://doi.org/10.1021/acsomega.2c01859
ACS Omega 2022, 7, 28849−28859

determined L value for each MC sample into eqs 1 and 2. Although the numbers of D_r data points are not sufficient to discuss the formation of the rigid rod particles in detail, the reasonable agreement between theory and experimental D_t (and D_r) data clearly observed in Figure 7a reveals that the MC samples form elongated rigid rodlike particles irrespective of M_w from the viewpoint of D_t data.

Viscometric Behaviors. The M_w dependence of $[\eta]$ for the MC samples dissolved in aqueous solution is shown in Figure 8 and Table 1. If one neglects the data of the longest

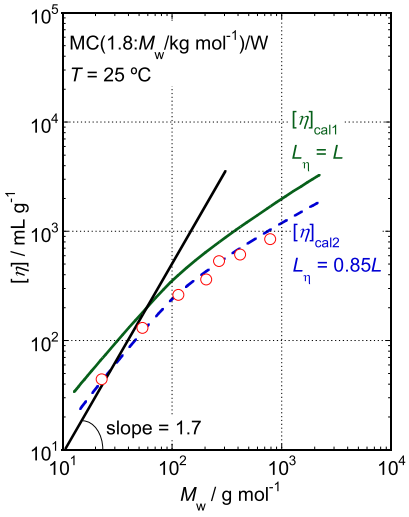

Figure 8. M_w dependence of $[\eta]$ for the MC samples dissolved in aqueous solution. The slope of the straight line is 1.7. Solid and broken curves indicate theoretical calculations using eq 3, assuming $L_\eta = L$ for $[\eta]_{cal1}$ and $L_\eta = 0.85L$ for $[\eta]_{cal2}$, respectively.

MC(1.8:790) sample, a Mark−Houwink−Sakurada-type expression such as $[\eta] \propto M_w^{0.9-1.0}$ can be approximately obtained forcibly. However, it seems that the classical Mark−Houwink−Sakurada expression does not fit our data as we observe a changing structure with increasing M_w, that is, the folding number, lL^{-1}, and particle diameter, d, change with increasing M_w, as discussed above. On the low M_w side, the $[\eta]$ data seem to have a large slope close to ca 1.7, that is, $[\eta] \propto M_w^{1.7}$, which is a typical value for rigid rod particles.[35,36] Therefore, we analyze the M_w dependence of the $[\eta]$ data based on the idea that rigid elongated rodlike particles are formed in this system.

According to the theoretical prediction, the intrinsic viscosity $[\eta]$ of rigid rod particles with the molar mass, M_w, length, L, and a diameter, d, is given using eq 3.[35,37]

$$[\eta] = \frac{2\pi N_A L^3}{45 M_w \{\ln(L/d) + C_\eta\}} \quad (3)$$

where N_A and C_η represent Avogadro's number and a numerical constant showing hydrodynamic interactions described by polynomials of the ratio L/d.[35] The solid line observed in Figure 8 demonstrates the M_w dependence of the theoretically calculated $[\eta]_{cal1}$ by directly substituting the L and d values determined by the SLS measurements into eq 3 at each M_w value. In the case of the examined MC samples, the L/d values were greater than 30 even for the shortest MC(1.8:23) sample. When the L/d value has such large numbers, the numerical parameter, C_η, approaches a constant value of ca −0.93.[35] We used the relationship $C_\eta = -0.93$ in this study. Although agreement between the theoretical solid line and experimental $[\eta]$ data is not as good, the solid line has a similar M_w dependence to that qualitatively observed in the $[\eta]$ data. On the other hand, the broken line, as shown in Figure 8, indicates the $[\eta]_{cal2}$ curve theoretically calculated via eq 3, assuming that the hydrodynamically effective particle length (L_η) is not identical to L but $0.85L$.[25] Because the agreement between the $[\eta]_{cal2}$ and $[\eta]$ data in Figure 8 appears reasonable, the presence of rodlike particles is certain in aqueous solutions of the examined MC samples. If $L_\eta = 0.85L$ is assumed via eqs 1 and 2, agreement between the theoretical calculations and data is reasonably maintained, as seen in Figure 7a,b. Therefore, it seems that hydrodynamically, the particle length behaves to be shorter than that determined by the SLS techniques by approximately 15%. A similar difference between the L_h and L values was also recently reported in PVDF/NMP solution systems, in which PVDF molecules form highly elongated rigid rodlike particles.[25] Consequently, the viscometric data, as well as other experimental techniques such as the SLS and DLS measurements, also revealed the formation of elongated rigid rodlike particles in the MC samples.

CONCLUSIONS

S-WANS experiments revealed that the local structure of MC ether samples with a DS of 1.8 dissolved in aqueous solution is reasonably explained with rodlike shape particles, in which MC molecular chains are elongated and folded to show weak periodicities of approximately 0.4 and 1.0 nm. The shorter spacing corresponds to the length of a structural repeating unit, cellobiose, and the other to the distance between facing molecular chain portions in the rodlike structure. The diameter, d, of the formed local rodlike structure increases gradually with increasing average molar mass, M_w.

The results of SLS and DLS measurements were rationally described with the idea that the rodlike local structure is extended to the overall particle structure of the MC samples dissolved in aqueous solution irrespective of M_w over the entire M_w range examined. Because the molecular chain folding number in the formed highly elongated rodlike particles is altered with increasing M_w, the M_w dependence of R_g does not follow the relationship $R_g \propto M_w$, which is valid in simple rigid rod particles for which lengths, L, are proportional to M_w. However, the formed particles have a rigid rodlike structure that clearly shows the evidential relationship $L^2 = 12R_g^2$ irrespective of M_w.

Reasonable agreement between the intrinsic viscosity, $[\eta]$, data, and the theoretical calculation, assuming the presence of rigid rods, also supports the formation of elongated rigid rodlike particles in the MC samples irrespective of M_w..

ASSOCIATED CONTENT

Supporting Information

The Supporting Information is available free of charge at https://pubs.acs.org/doi/10.1021/acsomega.2c01859.

Procedures to determine $\sqrt{KcR_\theta^{-1}}_{c=0}$ ($= \lim_{c\to 0}\sqrt{KcR_\theta^{-1}}$) data at each q value for some typical MC samples dissolved in aqueous solution and dependencies of $\sqrt{KcR_\theta^{-1}}_{c=0}$ data on q^2 and $\sqrt{KcR_\theta^{-1}}_{q=0}$ on c for aqueous solutions of MC samples at 25 °C other than MC(1.8:270) (PDF)

https://doi.org/10.1021/acsomega.2c01859
ACS Omega 2022, 7, 28849−28859

AUTHOR INFORMATION

Corresponding Author

Toshiyuki Shikata − *Cellulose Research Unit and Division of Natural Resources and Eco-materials, Graduate School of Agriculture, Tokyo University of Agriculture and Technology, Fuchu, Tokyo 183-8509, Japan;* orcid.org/0000-0001-6846-4985; Email: shikata@cc.tuat.ac.jp

Authors

Erika Saiki − *Cellulose Research Unit and Division of Natural Resources and Eco-materials, Graduate School of Agriculture, Tokyo University of Agriculture and Technology, Fuchu, Tokyo 183-8509, Japan*

Misato Yoshida − *Cellulose Research Unit and Division of Natural Resources and Eco-materials, Graduate School of Agriculture, Tokyo University of Agriculture and Technology, Fuchu, Tokyo 183-8509, Japan*

Kei Kurahashi − *Cellulose Research Unit and Division of Natural Resources and Eco-materials, Graduate School of Agriculture, Tokyo University of Agriculture and Technology, Fuchu, Tokyo 183-8509, Japan*

Hiroki Iwase − *Neutron Science and Technology Center, Comprehensive Research Organization for Science and Society (CROSS), Tokai, Ibaraki 319-1106, Japan;* orcid.org/0000-0003-4038-7839

Complete contact information is available at: https://pubs.acs.org/10.1021/acsomega.2c01859

Notes

The authors declare no competing financial interest.

ACKNOWLEDGMENTS

All the MC ether samples examined in this study were kindly supplied by Shin-Etsu Chemical Co. Ltd. (Tokyo), and this work was partially supported by the same company. We would like to thank Shingo Niinobe of Shin-Etsu Chemical Co. Ltd. and Dr. Kazuhisa Hayakawa, who previously worked for the same company, for their kind collaboration on this study. The S-WANS experiments at the Materials and Life Science Experimental Facility of the J-PARC were performed under a user program (Proposal no. 2020A00158).

REFERENCES

(1) Klemm, D.; Heublein, B.; Fink, H.-P.; Bohn, A. Cellulose: Fascinating Biopolymer and Sustainable Raw Material. *Angew. Chem., Int. Ed.* **2005**, *44*, 3358−3393.

(2) Nishiyama, Y.; Langan, P.; Chanzy, H. Crystal Structure and Hydrogen-Bonding System in Cellulose Iβ from Synchrotron X-ray and Neutron Fiber Diffraction. *J. Am. Chem. Soc.* **2002**, *124*, 9074−9082.

(3) Nishiyama, Y.; Sugiyama, J.; Chanzy, H.; Langan, P. Crystal Structure and Hydrogen Bonding System in Cellulose Iα from Synchrotron X-ray and Neutron Fiber Diffraction. *J. Am. Chem. Soc.* **2003**, *125*, 14300−14306.

(4) Li, Y.; Liu, X.; Zhang, Y.; Jiang, K.; Wang, J.; Zhang, S. Why Only Ionic Liquids with Unsaturated Heterocyclic Cations Can Dissolve Cellulose: A Simulation Study. *ACS Sustainable Chem. Eng.* **2017**, *5*, 3417−3428.

(5) Kamide, K. *Cellulose and Cellulose Derivatives; Molecular Characterization and its Applications*; Elsevier: Amsterdam, 2005; Chapter. 2&3.

(6) Klemm, D.; Philipp, B.; Heinze, T., Heinze, U.; Wagenknecht, W. *Comprehensive Cellulose Chemistry: Volume 2 Functionalization of Cellulose*; Wiley-VCH Verlag GmbH: Weinheim: 1998: Chapter 4.

(7) Wuestenberg, T. *Cellulose and Cellulose Derivatives in the Food Industry: Fundamentals and Applications*; John Wiley & Sons, 2014; Chapter 5.

(8) Knapen, E.; Van Gemert, D. Cement hydration and microstructure formation in the presence of water-soluble polymers. *Cem. Concr. Res.* **2009**, *39*, 6−13.

(9) Seddiqi, H.; Oliaei, E.; Honarkar, H.; Jin, J.; Geonzon, L. C.; Bacabac, R. G.; Klein-Nulend, J. Cellulose and its derivatives: towards biomedical applications. *Cellulose* **2021**, *28*, 1893−1931.

(10) Podczeck, F.; Jones, B. *Pharmaceutical Capsules*, 2nd ed.; Pharmaceutical Press: London, 2004; Chapter 3.

(11) Saito, M. Wormlike Chain Parameters of Cellulose and Cellulose Derivatives. *Polym. J.* **1983**, *15*, 213−223.

(12) Lodge, T. P.; Maxwell, A. L.; Lott, J. R.; Schmidt, P. W.; McAllister, J. W.; Morozova, S.; Bates, F. S.; Li, Y.; Sammler, R. L. Gelation, Phase Separation, and Fibril Formation in Aqueous Hydroxypropylmethylcellulose Solutions. *Biomacromolecules* **2018**, *19*, 816−824.

(13) McAllister, J. W.; Schmidt, P. W.; Dorfman, K. D.; Lodge, T. P.; Bates, F. S. Thermodynamics of Aqueous Methylcellulose Solutions. *Macromolecules* **2015**, *48*, 7205−7215.

(14) Keary, C. M. Characterization of METHOCEL cellulose ethers by aqueous SEC with multiple detectors. *Carbohydr. Polym.* **2001**, *45*, 293−303.

(15) Arai, K.; Horikawa, Y.; Shikata, T.; Iwase, H. Reconsideration of the conformation of methyl cellulose and hydroxypropyl methyl cellulose ethers in aqueous solution. *RSC Adv.* **2020**, *10*, 19059−19066.

(16) Bodvik, R.; Dedinaite, A.; Karlson, L.; Bergström, M.; Bäverbäck, P.; Pedersen, J. S.; Edwards, K.; Karlsson, G.; Varga, I.; Claesson, P. M. Aggregation and network formation of aqueous methylcellulose and hydroxypropylmethylcellulose solutions. *Colloids Surf., A* **2010**, *354*, 162−171.

(17) Morozova, S. Methylcellulose fibrils: a mini review. *Polym. Int.* **2020**, *69*, 125−130.

(18) Coughlin, M. L.; Liberman, L.; Ertem, S. P.; Edmund, J.; Bate, F. S.; Lodge, T. Methyl cellulose solutions and gels: fibril formation and gelation properties. *Prog. Polym. Sci.* **2021**, *112*, 101324.

(19) Arai, K.; Shikata, T. Hydration/Dehydration Behavior of Cellulose Ethers in Aqueous Solution. *Macromolecules* **2017**, *50*, 5920−5928.

(20) Takata, S.; Suzuki, J.; Shinohara, T.; Oku, T.; Tominaga, T.; Ohishi, K.; Iwase, H.; Nakatani, T.; Inamura, Y.; Ito, T.; Suzuki, K.; Aizawa, K.; Arai, M.; Otomo, T.; Sugiyama, M. The Design and q Resolution of the Small and Wide Angle Neutron Scattering Instrument (TAIKAN) in J-PARC. *JPS Conf. Proc.* **2015**, *8*, 036020.

(21) Fournet, G. Étude théorique et expérimentale de la diffusion des rayons X par les ensembles denses de particules. *Bull. Mineral.* **1951**, *74*, 37−172.

(22) Doucet, M. et al. *SasView Version 5.0.3, Zenodo*, 2021, https://www.sasview.org/.

(23) Chatterjee, T.; Nakatani, A. I.; Adden, R.; Brackhagen, M.; Redwine, D.; Shen, H.; Li, Y.; Wilson, T.; Sammler, R. L. Structure and Properties of Aqueous Methylcellulose Gels by Small-Angle Neutron Scattering. *Biomacromolecules* **2012**, *13*, 3355−3369.

(24) Langan, P.; Nishiyama, Y.; Chanzy, H. X-ray Structure of Mercerized Cellulose II at 1 Å Resolution. *Biomacromolecules* **2001**, *2*, 410−416.

(25) Nohara, Y.; Saiki, E.; Shikata, T. Long Two-Dimensional Folding Chain Structure Formation of Poly(vinylidene fluoride) in Solutions of a Polar Solvent, *N*-Methylpyrrolidone. *ACS Appl. Polym. Mater.* **2022**, *4*, 1255−1263.

(26) Huang, W.; Dalal, I. S.; Larson, R. G. Analysis of Solvation and Gelation Behavior of Methylcellulose Using Atomistic Molecular Dynamics Simulations. *J. Phys. Chem. B* **2014**, *118*, 13992−14008.

(27) Glatter, O. *Scattering Methods and their Application in Colloid and Interface Science*; Elsevier: Amsterdam; 2018, Chapters 9 & 10.

(28) Berry, G. C. Thermodynamic and Conformational Properties of Polystyrene. I. Light-Scattering Studies on Dilute Solutions of Linear Polystyrenes. *J. Chem. Phys.* **1966**, *44*, 4550−4564.
(29) Zimm, H. B. The Scattering of Light and the Radial Distribution Function of High Polymer Solutions. *J. Chem. Phys.* **1948**, *16*, 1093−1099.
(30) Nayuk, R.; Huber, K. Formfactors of Hollow and Massive Rectangular Parallelepipeds at Variable Degree of Anisometry. *Z. Phys. Chem.* **2012**, *226*, 837−854.
(31) Berne, B.; Pecora, R. *Dynamic Light Scattering*; Wiley: New York, 1976; Chapter 8.
(32) Schillen, K.; Brown, W.; Johnsen, R. M. Micellar Sphere-to-Rod Transition in an Aqueous Triblock Copolymer System. A Dynamic Light Scattering Study of Translational and Rotational Diffusion. *Macromolecules* **1994**, *27*, 4825−4832.
(33) Arai, K.; Horikawa, Y.; Shikata, T. Transport Properties of Commercial Cellulose Nanocrystals in Aqueous Suspension Prepared from Chemical Pulp via Sulfuric Acid Hydrolysis. *ACS Omega* **2018**, *3*, 13944−13951.
(34) Hasegawa, H.; Horikawa, Y.; Shikata, T. Cellulose Nanocrystals as a Model Substance for Rigid Rod Particle Suspension Rheology. *Macromolecules* **2020**, *53*, 2677−2685.
(35) Ortega, A.; García de la Torre, J. Hydrodynamic properties of rodlike and disklike particles in dilute solution. *J. Chem. Phys.* **2003**, *119*, 9914−9919.
(36) Yanaki, T.; Norisuye, T.; Fujita, H. Triple Helix of Schirophyllum commune Polysaccharide in Dilute Solution. 3. Hydrodynamic Properties in Water. *Macromolecules* **1980**, *13*, 1462−1466.
(37) Dio, M.; Edwards, S. F. *The Theory of Polymer Dynamics*; Clarendon Press: Oxford, 1986; Chapter 8.

https://doi.org/10.1021/acsomega.2c01859
ACS Omega 2022, 7, 28849−28859